Scientific Review – Engineering and Environmental Sciences (2019), 28 (3), 345–355
Sci. Rev. Eng. Env. Sci. (2019), 28 (3)
Przegląd Naukowy – Inżynieria i Kształtowanie Środowiska (2019), 28 (3), 345–355
Prz. Nauk. Inż. Kszt. Środ. (2019), 28 (3)
http://iks.pn.sggw.pl
DOI 10.22630/PNIKS.2019.28.3.32

Krzysztof GROMYSZ, Mateusz SMOLANA
Faculty of Civil Engineering, Silesian University of Technology

Examination of stiffness of stack of steel elements forming part of supports used for removal of building deflections

Key words: stack of elements, stiffness, mining subsidence, removal of building deflections

Introduction

The removal of building deflections consists of uneven raising of buildings with piston hydraulic jacks (Gromysz, 2017). The jack piston extension is limited to 200 mm. If the height of raising a building exceeds this value, it is necessary to periodically underlay the jacks with elements increasing the lifting range. This way, a temporary support is created, consisting of a hydraulic jack, a stack of parallelepiped elements located under the jack and frequently also additional plates (Fig. 1).

The mechanical properties of the stack of elements situated under the jack dictate the properties of the temporary support. In particular, support stiffness depends to the greatest extent on the stack stiffness.

Subject to investigations up till now have been only the parameters of a stack of wooden elements used for elimination of deflections of low structures, with up

FIGURE 1. Rectification process scheme and temporary supports

to three stories (Gromysz, 2018). Moreover, the analyses of axially and eccentrically loaded elements have been carried out mainly in relation to reinforced concrete elements (Kabir & Shafei, 2012), steel columns (Nie, Kang, Shen & Yang, 2017) and masonry structures (Bernat-Maso, Gil & Roca, 2015; Moradabadi, Laefer, Clarke & Lourenço, 2015). Respectively, the results of the experimental research concerns mainly glass fibre reinforced polymer-reinforced geopolymer concrete – GFRP-RGC (Elchalakani, Karrech, Dong, Ali & Yang, 2018), steel (Nie et al., 2017), masonry structures (Cavaleri, Failla, Mendola & Papia, 2005; Bernat-Maso, Gil & Escrig, 2015) and composite multi-drum columns (Buzov, Radnić, Grgić & Baloević, 2018).

This paper presents the results of tests of a stack of parallelepiped steel elements used for the removal of deflections of high buildings.

Temporary support

The subject of the analysis is a stack of unconnected cuboidal elements with the total length of l_{st} = 1.0 m, forming part of the support (Fig. 2). A single element of the stack consists of rolled profiles joined by welding (Fig. 2). The entire support together with a jack will be subject to experimental tests to reflect the actual working conditions of the stack.

In real conditions, the support rests upon the prepared substrate, so the base of support is not displaced or rotated. A piston of a hydraulic jack is ended with a swivel saddle. It can thus be concluded that a static scheme of the support is represented by a one-end-fixed column, loaded with the force Q_z (Fig. 2).

The stiffness of the support $k_{sup,z}$ in the vertical direction, understood as the value of the force Q_z divided by the change Δl_{sup} of its length, results from the serial connection of the jack with the longitudinal stiffness $k_{hj,z}$ and stack $k_{st,z}$. As presented above, a stack of steel elements will be the subject of the analysis only.

Stack stiffness results from the serial connection of n single parallelepiped elements with stiffness $k_{cub,z}$ each. In order to determine the theoretical stiffness $k_{st,z,teor,1m}$ of the stack with the length l_{st} = 1.0 m, the stiffness $k_{cub,z}$ of one element should hence be first calculated,

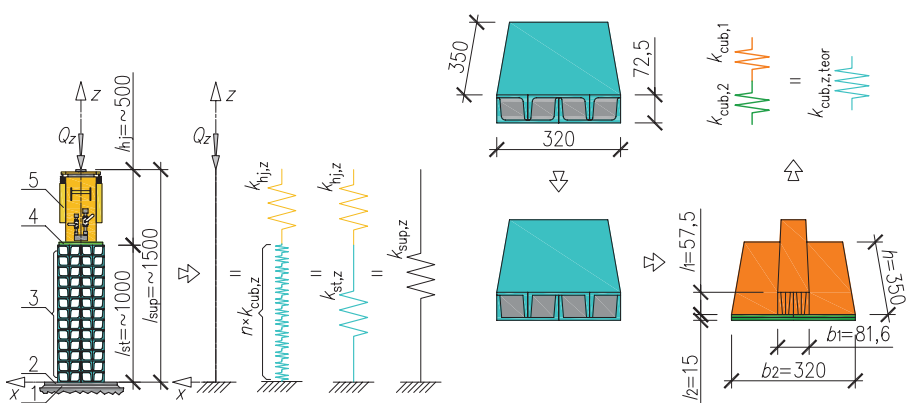

FIGURE 2. Static scheme of the support and parallelepiped element

and then n elements should be connected serially. The stiffness of a single parallelepiped element, due to its cross section changing in a stepwise manner, is determined with consideration of two stiffnesses, i.e. $k_{\mathrm{cub},1}$ and $k_{\mathrm{cub},2}$ (Fig. 2)

$$k_{\mathrm{cub},i} = \frac{h_i \cdot b_i \cdot E}{l_i} \tag{1}$$

where:
h_i, b_i, l_i – dimensions presented in Figure 2;
E – Young's modulus of S235 steel (210 GPa).

Hence the stiffness of one parallelepiped element determined from the dependence (2)

$$k_{\mathrm{cub},z,\mathrm{teor}} = \frac{k_{\mathrm{cub},1} k_{\mathrm{cub},2}}{k_{\mathrm{cub},1} + k_{\mathrm{cub},2}} \tag{2}$$

is 97,800.2 kN·mm^{-1}.

In turn, the theoretical stiffness $k_{\mathrm{st},z,\mathrm{teor},1\mathrm{m}}$ of the stack n = 13 of elements forming a stack with the length l_{st} = 1 m, resulting from the serial connection of elements, determined from the formula (3)

$$k_{\mathrm{st},z,\mathrm{teor},1\mathrm{m}} = \frac{k_{\mathrm{cub},z,\mathrm{teor}}}{n} \tag{3}$$

equals 7,523.1 kN·mm^{-1}.

Examination of stack stiffness

As mentioned above, the aim of the conducted tests is to determine the stiffness $k_{\mathrm{st},z,1\mathrm{m}}$ of a stack with the length l_{st} = = 1 m, consisting of 13 parallelepiped elements. This stiffness was defined as the change the force Q_z value divided by the corresponding change of the stack length:

$$k_{\mathrm{st},z,1\mathrm{m}} = \frac{Q_z}{\Delta l_{\mathrm{st}}} \tag{4}$$

The observations made when removing the deflections of objects show, that stack stiffness depends on the value of the load Q_z and on the load phase. Moreover, due to the fact that a stack of unconnected elements is being loaded, stiffness under the increasing load is different than under the lowering load. A program of tests was therefore created in which supports are loaded with the increasing and decreasing force Q_z.

Test stand

It is impossible to reproduce in laboratory conditions the conditions similar to real conditions, where a stack would be loaded with gravity force with the value of up to 1,000 kN, while ensuring the freedom of stack deformations and jack head displacements in all three directions. It was therefore necessary to apply a substitute scheme. The actual support, wherein the static scheme is a one-end--fixed column with the length l_{sup}, was replaced by a system consisting of two supports directed to each other with bases (Fig. 3). A simply supported system with the length $2l_{\mathrm{sup}}$ was therefore examined. The character of the actual support's behaviour, shown in Figure 3, was maintained here without the need to ensure the free displacement of the loaded end of the element. It was only necessary to ensure its rotation.

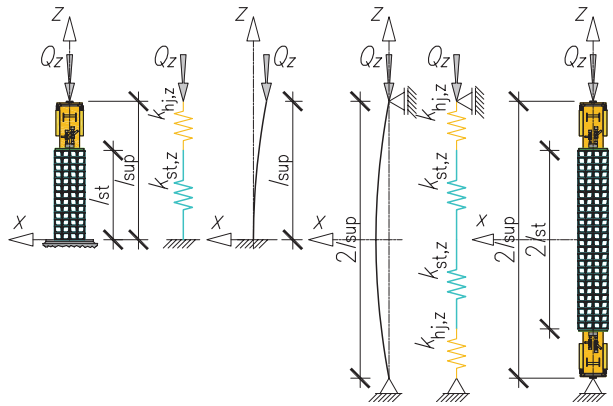

FIGURE 3. Substitute scheme of the tested support

The system mentioned was installed in a horizontal position on a test stand (Fig. 4). Support was provided under each of the elements in the form of bearings moving along a polished steel plate. Movement resistance was minimized this way and the freedom of deformations along the axis z, of displacements along the axis x and of rotations along the axis y are ensured for the entire examined system.

A measuring system consisting of a force transducer, LVDT sensors, computer with software, designed for data acquisition, and an analogue-to-digital converter, was applied for measuring displacements and forces. The measurement accuracy of forces and displacements was 1%.

Programme and progress of tests

A system with the length of $2l_{st} = 2.0$ m (Fig. 4), loaded with the cyclic force Q_z, was tested. The load was changed from zero to the maximum value $Q_{z,max}$.

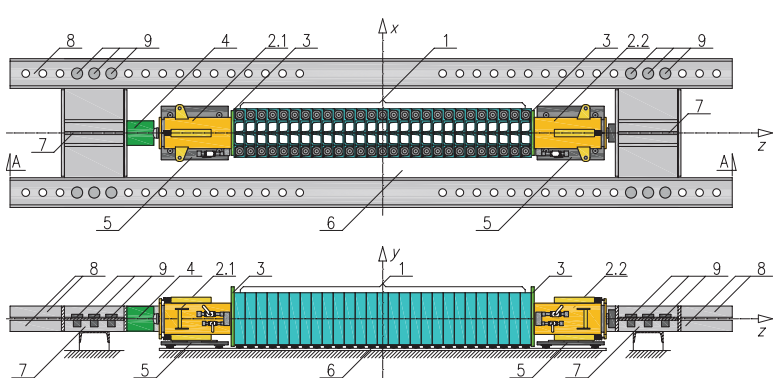

FIGURE 4. Test stand with the tested system: top view and cross-section A–A: 1 – stack of 27 parallelepiped elements; 2.1 – passive hydraulic jack; 2.2 – active hydraulic jack; 3 – steel plate; 4 – force transducer; 5 – trolley of hydraulic jack; 6 – polished stainless steel plate; 7 – head of the stand; 8 – ties; 9 – steel bolts

Seven $Q_{z,\max}$ values were adopted, equal to: 50, 75, 100, 250, 500, 750, 1,000 kN. Seven tests of the system were altogether carried out, with four load – unload cycles in each test. Twenty seven hysteresis loops were obtained this way. The force Q_z was changing during the test with the rate of about 20 kN·s^{-1}, which corresponds to actual conditions during building's rectification. The designations of successive tests together with successive values of the force Q_z are shown in Table 1. The longitudinal force Q_z and variations in the length of the sections $2\Delta l_{st,1}$ and $2\Delta l_{st,2}$ (Fig. 5) were measured during the tests.

Tests results and their analysis

Course of the dependence $Q_z - \varepsilon_{st,z}$

The length change of the examined stack with the original length $2l_{st}$ is calculated based on the measured changes in the length of sections $2\Delta l_{st,1}$ and $2\Delta l_{st,2}$ according to the formula

$$2\Delta l_{st} = \frac{2\,\Delta l_{st,1} + 2\,\Delta l_{st,2}}{2} \tag{5}$$

Stack deformation $\varepsilon_{st,z}$ was defined as

$$\varepsilon_{st,z} = \frac{2\Delta l_{st}}{2l_{st}} \tag{6}$$

TABLE 1. Designations of tests and range of loads implemented in individual tests

Test designation	Successive values of the force – Q_z [kN]
st/2000/0/0-50/comp	0→50→0→50→0→50→0→50→0
st/2000/0/0-75/comp	0→75→0→75→0→75→0→75→0
st/2000/0/0-100/comp	0→100→0→100→0→100→0→100→0
st/2000/0/0-250/comp	0→250→0→250→0→250→0→250→0
st/2000/0/0-500/comp	0→500→0→500→0→500→0→500→0
st/2000/0/0-750/comp	0→750→0→750→0→750→0→750→0
st/2000/0/0-1000/comp	0→1 000→0→1 000→0→1 000→0→1 000→0

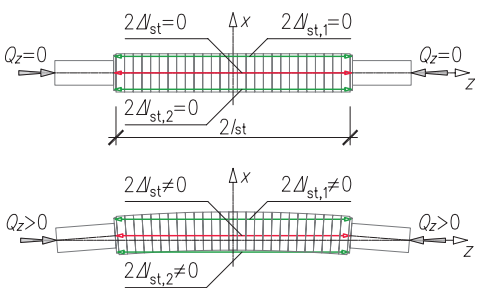

FIGURE 5. Measurement points

Figure 6 show four full load-unload cycles obtained as a result of the carried out tests st/2000/0/0-50/comp (a test corresponding to the smallest value of the force $Q_{z,\max} = 50$ kN) and st/2000/0/0--1000/comp (a test corresponding to the highest value of the force $Q_{z,\max} = 1{,}000$ kN). The analogous cycles were obtained for all the tests corresponding to the values $Q_{z,\max}$.

The hysteresis loops $Q_z - \varepsilon_{st,z}$, corresponding to all four cycles in a given test, are coinciding, so one of them was only presented below. The superimposed

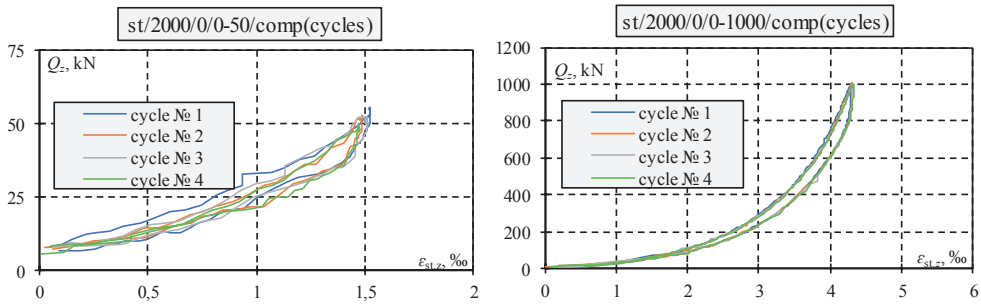

FIGURE 6. Four hysteresis loops

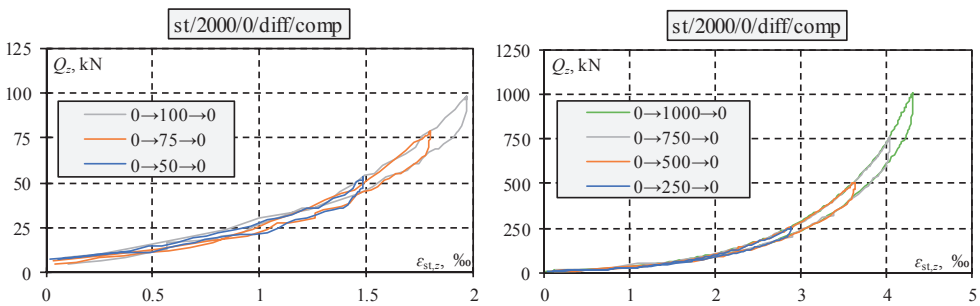

FIGURE 7. Single hysteresis loops from different tests

courses of loops from all the tests are presented in Figure 7.

The courses of graphs of the function $Q_z - \varepsilon_{st,z}$ obtained in all the tests are coinciding in the common ranges of the load. The phases (Fig. 7) can be distinguished in all the tests on the charts $Q_z - \varepsilon_{st,z}$. The first phase corresponds to the monotonic increase in the load from zero to $Q_{z,\max}$. The dependence $Q_z - \varepsilon_{st,z}$ in this phase is non-linear because there is a clear increase in the slope of the curve along with the rising load. During unloading, the linear dependence $Q_z - \varepsilon_{st,z}$ is first observed. Then, along with a further decrease in the load, the non-linear dependence $Q_z - \varepsilon_{st,z}$ is observed because along with the falling Q_z, the slope of the curve $Q_z - \varepsilon_{st,z}$ decreases. Based on such observations, in order to conduct a further analysis, it was decided to divide the hysteresis loop $Q_z - \varepsilon_{st,z}$ to three phases, as shown in Figure 8. The following was therefore distinguished.

Phase I of the load with the non-linear dependence $\varepsilon_{st,z} - Q_z$. The load is rising here from zero to $Q_{z,\max}$ and the deformation to the value $\varepsilon_{st,z,\max}$.

Phase II of unloading with the linear dependence $\varepsilon_{st,z} - Q_z$. The load value decreases to $Q_{z,\max}$ from the agreed limit

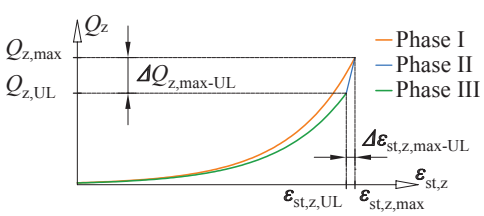

FIGURE 8. Phases in the load-unload cycle

$Q_{z,\mathrm{UL}}$. The value $Q_{z,\mathrm{UL}}$ was read from charts and was between 0.70 to 0.82 of the value $Q_{z,\max}$. The strain changed from $\varepsilon_{\mathrm{st},z,\max}$ to the agreed limit of $\varepsilon_{\mathrm{st},z,\mathrm{UL}}$.

Phase III including the unloading process, in which the graph $\varepsilon_{\mathrm{st},z} - Q_z$ has a non-linear course. The load value decreases from $Q_{z,\mathrm{UL}}$ to zero, and deformation from $\varepsilon_{\mathrm{st},z,\mathrm{UL}}$ to zero.

The values of forces Q_z and of deformations $\varepsilon_{\mathrm{st},z}$, being the limits of particular phases, are presented in Table 2.

was approximated with the function f_{III} in the form (9).

$$f_{\mathrm{I}} : Q_z(\varepsilon_{\mathrm{st},z}) = \alpha_{\mathrm{I}} e^{\beta_{\mathrm{I}} \varepsilon_{\mathrm{st},z}} \tag{7}$$

$$f_{\mathrm{II}} : Q_z(\varepsilon_{\mathrm{st},z}) = \alpha_{\mathrm{II}} \varepsilon_{\mathrm{st},z} + \beta_{\mathrm{II}} \tag{8}$$

$$f_{\mathrm{III}} : Q_z(\varepsilon_{\mathrm{st},z}) = \alpha_{\mathrm{III}} e^{\beta_{\mathrm{III}} \varepsilon_{\mathrm{st},z}} \tag{9}$$

The coefficients α_{I}, α_{III} and β_{I}, β_{III} were determined with the least squares method. In turn, the coefficients α_{II} and

TABLE 2. Limits of phases

Test designation	$Q_{z,\max}$ [kN]	$\varepsilon_{\mathrm{st},z,\max}$ [‰]	$Q_{z,\mathrm{UL}}$ [kN]	$\varepsilon_{\mathrm{st},z,\mathrm{UL}}$ [‰]
st/2000/0/0-50/comp	52.92	1.485	39.20	1.419
st/2000/0/0-75/comp	79.50	1.796	65.63	1.774
st/2000/0/0-100/comp	98.33	1.969	79.33	1.928
st/2000/0/0-250/comp	249.78	2.872	204.39	2.832
st/2000/0/0-500/comp	507.12	3.625	413.76	3.590
st/2000/0/0-750/comp	757.03	4.035	599.70	3.993
st/2000/0/0-1000/comp	1 008.27	4.315	807.57	4.273

The courses of the dependence $Q_z - \varepsilon_{\mathrm{st},z}$ of successive phases can be approximated with successive approximation functions f_i. Phase I was approximated with the function f_{I} in the form (7), phase II was approximated with the function f_{II} in the form (8) and Phase III

β_{II} were determined by creating an equation for a straight line coming through two points which constituted the limit of phases I and III.

Figure 9 shows the examples of graphs of the function f_i superimposed on the results of experimental tests:

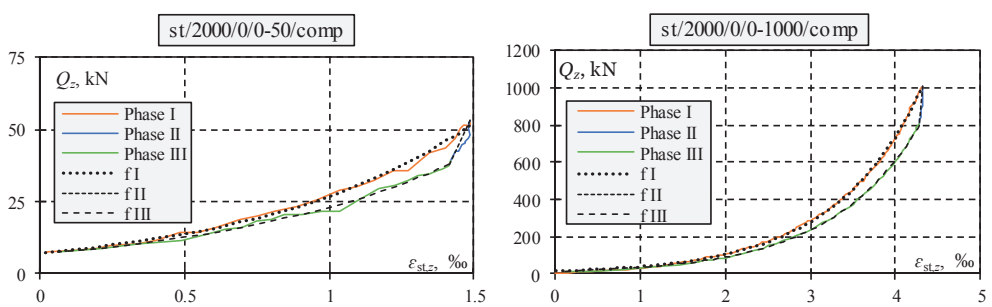

FIGURE 9. Phases I–III and approximation functions f_{I}–f_{III}

st/2000/0/0-50/comp (a test corresponding to the smallest value of the force $Q_{z,\max}$ = 50 kN) and st/2000/0/0-1000/ /comp (a test corresponding to the highest value of the force $Q_{z,\max}$ = 1,000 kN). The analogous graphs can be of course created for all the tests. Satisfactory consistency of tests results with the description of the dependencies (7), (8), (9) is seen here.

Stack stiffness $k_{st,z}$

As a result of deriving the functions f_i approximating the courses of the dependencies $Q_z - \varepsilon_{st,z}$, the dependencies (10) are obtained describing the stiffnesses $k_{st,z,i}$ as the functions of strains.

$$k_{st,z,i}(\varepsilon_{st,z}) = \frac{\mathbf{d}f_i}{\mathbf{d}\varepsilon_{st,z}} \tag{10}$$

Hence the functions of stiffness in particular phases have the forms

$$k_{st.z,I}(\varepsilon_{st,z}) = \alpha_I \beta_I e^{\beta_I \varepsilon_{st,z}} \tag{11}$$

$$k_{st,z,II}(\varepsilon_{st,z}) = \alpha_{II} \tag{12}$$

$$k_{st,z,III}(\varepsilon_{st,z}) = \alpha_{III} \beta_{III} e^{\beta_{III} \varepsilon_{st,z}} \tag{13}$$

The reverse functions f_I^{-1} and f_{III}^{-1} were determined to examine the effect of the load value on stack stiffness.

$$f_i^{-1} = \varepsilon_{st,z}(Q_z) = \frac{\ln\left(\frac{Q_z}{\alpha_i}\right)}{\beta_i}, \; i = \text{I, III} \tag{14}$$

The dependence (14) describes the strain $Q_{st,z}$ as the function of the load Q_z. The following dependence (15) is obtained after substituting (14) to the equations (11) and (13):

$$k_{st,z,i}(Q_z) = \alpha_i \beta_i e^{\beta_i \frac{\ln\left(\frac{Q_z}{\alpha_i}\right)}{\beta_i}}, \quad i = \text{I, III} \tag{15}$$

which, after transformation, assumes the form

$$k_{st,z,i}(Q_z) = B_i Q_z, \; i = \text{I, III} \tag{16}$$

It turns out that the stiffnesses $k_{st,z,I}$ and $k_{st,z,III}$ of the stack are the linear functions of the load Q_z. The stiffness is therefore proportional to the load and increases along with the increasing load force. At the same time, the directional coefficients of the dependence (16) are equal to the coefficients β_I and β_{III} – determined with the least squares method – of, respectively, functions f_I and f_{III}.

The derived function $k_{st,z,II}$ has the constant value α_{II} in phase II and seems to be independent from the variable Q_z. This constant assumes however different values depending on the value of the maximum force $Q_{z,\max}$. It turns out that in the analysed load range of $Q_{z,\max}$, stack stiffness in phase II varies approximately linearly in accordance with equation (17).

$$k_{st,z,II}(Q_{z,\max}) = 4{,}487 \; Q_{z,\max} \tag{17}$$

where:
$Q_{z,\max}$ – maximum load [kN];
$k_{st,z,II}$ – stiffnes in phase II [kN·‰$^{-1}$].

Figures from 10 to 12 show graphs of the stiffness $k_{st,z,I}$ from the load Q_z over the successive phases.

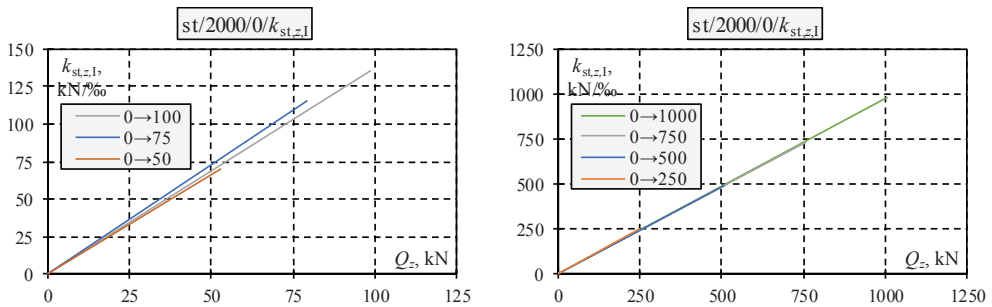

FIGURE 10. Stack stiffness variation in phase I according to the load Q_z

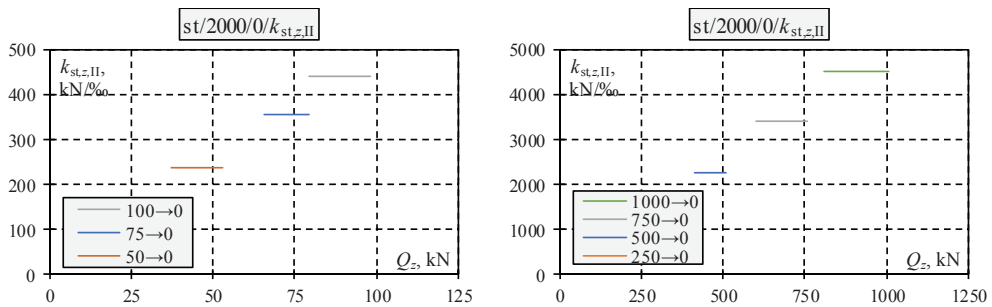

FIGURE 11. Stack stiffness variation in phase II according to the load Q_z

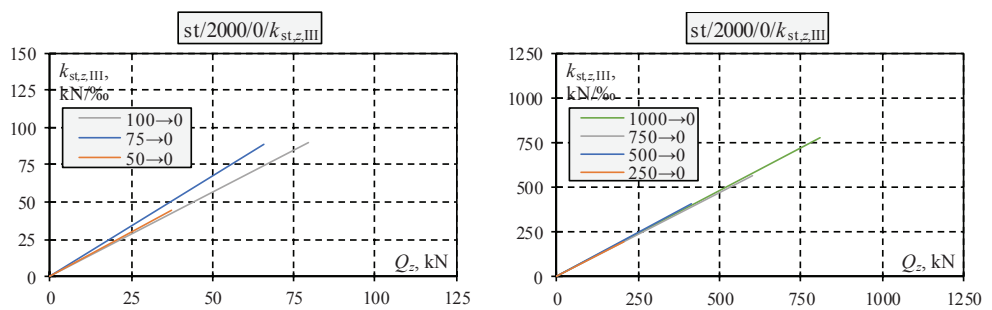

FIGURE 12. Stack stiffness variation in phase III according to the load Q_z

The maximum stiffnesses $k_{st,z,max,I}$ for all the phases were achieved for the highest load with the force Q_z.

After conducting the tests and describing them it is possible to compare the values of stack stiffness determined theoretically with the dependencies prepared on the basis of the tests. The theoretical analysis shows that stiffness $k_{st,z,teor}$ of the stack with the length of l_{st} = = 1 m, consisting of n = 13 elements is constant and equals 7,523.1 kN·mm^{-1} (the value determined on the basis of eq. 3). It was revealed by analysing the results of tests however that the stiffness is not a constant value and depends on the value of the load Q_z. Table 3 lists maximum stiffnesses corresponding to

three phases for the load Q_{max} = 1,000 kN, determined on the basis of the dependence (15), (16) and (17). The values were then compared, calculated according to equations (16) and (17), with the one determined according to equation (3), by introducing the parameter

$$\eta_{k,\mathrm{st},z} = \frac{k_{\mathrm{st},z,i}}{k_{\mathrm{st},z,\mathrm{teor}}} \cdot 100\% \qquad (18)$$

The values of this parameter are provided in the last column of Table 3.

It is seen by analysing the values provided in the Table 3 that the stiffnesses determined in experimental tests are even ten times smaller than the stiffnesses determined by calculations. This difference results from the deformations that occur at the interface between parallelepiped elements and deformations of the elements forming the stack. The deformations at the interface of elements result from the fact that the contact surface is not a perfect plane. In turn, higher deformations of the parallelepiped elements themselves result probably from the susceptibility of welding joints connecting the rolled parts, from which the parallelepiped elements were made.

rary building supports to correctly model the building deflection removal process. During the rectification, the stack forming part of the temporary support is loaded in a cyclic manner. Tests were designed and carried out for this reason, in which a stack of parallelepiped elements was loaded with the increasing and decreasing axial force Q_z.

Three distinct phases of the $Q_z - \varepsilon_{\mathrm{st},z}$ dependence course were identified in each of the conducted load – unload cycle tests. The loading process was described with one phase (phase I), whereas the unloading process with two phases (phases II and III).

The stack stiffness for the examined range of loads was not constant. The stiffness in phases I and III was varying in a linear manner along with the change of the load Q_z. In phase II, stiffness is indeed constant, however, its value depends on the value $Q_{z,\max}$, from which unloading takes place. This dependence is also linear.

The highest stack stiffness in all the phases was achieved during the test designated as st/2000/0/0-1000/comp, where $Q_{z,\max}$ reached the value of 1,008.3 kN. Such stiffnesses were, respectively, 13.1, 63.1 and 10.1% of the theoretical stiffness.

TABLE 3. Comparison of stiffnesses

Phase	Q_z [kN]	$k_{\mathrm{st},z,\max,i}$ [kN·‰$^{-1}$]	$k_{\mathrm{st},z,\mathrm{teor}}$ [kN·‰$^{-1}$]	$\eta_{k,\mathrm{st},z}$ [%]
I	1 008.3	983.1	7 523.1	13.1
II	1 008.3–807.6	4 750.1	7 523.1	63.1
III	807.6	762.2	7 523.1	10.1

Conclusions

It is critical to determine correctly the stiffness of the stack of steel parallelepiped elements forming part of tempo-

A non-linear behaviour of the stack results from its untypical construction. The elements of the stack are not permanently interconnected, and their coopera-

tion takes place by the contact of uneven surfaces. Investigations into the effect of eccentric setting of a hydraulic jack and of stack length on stack stiffness are currently pursued.

References

Bernat-Maso, E., Gil, L. & Roca, P. (2015). Numerical analysis of the load-bearing capacity of brick masonry walls strengthened with textile reinforced mortar and subjected to eccentric compressive loading. *Engineering Structures*, *91*, 96-111. doi: 10.1016/j.engstruct.2015.02.032

Bernat-Maso, E., Gil, L. & Escrig, C. (2015). Analysis of brick masonry walls strengthened with fibre reinforced polymers and subjected to eccentric compressive loads. *Construction and Building Materials*, *84*, 169-183. doi: 10.1016/j.conbuildmat.2015.02.078

Buzov, A., Radnić, J., Grgić, N. & Baloević, G. (2018). Effect of the drum height on the bearing capacity of composite multi-drum column under static load. *Composites Part B: Engineering*, *148*, 243-251. doi:10.1016/j.compositesb.2018.05.005

Cavaleri, L., Failla, A., Mendola, L.L. & Papia, M. (2005). Experimental and analytical response of masonry elements under eccentric vertical loads. *Engineering Structures*, *27*(8), 1175--1184. doi: 10.1016/j.engstruct.2005.02.012

Elchalakani, M., Karrech, A., Dong, M., Ali, M.M. & Yang, B. (2018). Experiments and Finite Element Analysis of GFRP Reinforced Geopolymer Concrete Rectangular Columns Subjected to Concentric and Eccentric Axial Loading. *Structures*, *14*, 273-289. doi: 10.1016/j.istruc.2018.04.001

Gromysz, K. (2017). Methods of Removing Buildings Deflection Used in Poland. *IOP Conference Series: Materials Science and Engineering*, *245*, 032096. doi:10.1088/1757-899x/245/3/032096

Gromysz, K. (2018). Deformations of temporary wooden supports used to reduce building deflections in mining areas. *E3S Web of Conferences*, *36*, 03002. doi: 10.1051/e3sconf/20183603002

Kabir, M.Z. & Shafei, E. (2012). Plasticity modeling of FRP-confined circular reinforced concrete columns subjected to eccentric axial loading. *Composites Part B: Engineering, 43*(8), 3497-3506. doi: 10.1016/j.compositesb.2011.11.075

Moradabadi, E., Laefer, D.F., Clarke, J. A. & Lourenço, P.B. (2015). A semi-random field finite element method to predict the maximum eccentric compressive load for masonry prisms. *Construction and Building Materials*, *77*, 489-500. doi: 10.1016/j.conbuildmat.2014.12.027

Nie, S., Kang, S., Shen, L. & Yang, B. (2017). Experimental and numerical study on global buckling of Q460GJ steel box columns under eccentric compression. *Engineering Structures*, *142*, 211-222. doi: 10.1016/j.engstruct.2017.03.064

Summary

Examination of stiffness of stack of steel elements forming part of supports used for removal of building deflections. The removal of building deflections consists of uneven raising of buildings with piston hydraulic jacks. A stack of parallelepiped steel elements is situated under jacks during deflection removal for technological reasons. The stack has decisive influence on the stiffness of the supports. Tests of the stack of parallelepiped elements loaded with increasing and decreasing force were designed and carried out. Three characteristic phases were identified based on the tests. The maximum stiffness in particular phases was, respectively 13.1, 63.1 and 10.1% of theoretical stiffness.

Author's address:
Krzysztof Gromysz
(https://orcid.org/0000-0002-7778-8620)
Mateusz Smolana
(https://orcid.org/0000-0001-6609-217X)
Politechnika Śląska
Wydział Budownictwa
ul. Akademicka 5, 44-100 Gliwice
Poland
e-mail: krzysztof.gromysz@polsl.pl